ResearchGate

See discussions, stats, and author profiles for this publication at: https://www.researchgate.net/publication/231654196

3D Gold Nanocrystal Arrays: A Framework for Reversible Lithium Storage

ARTICLE *in* THE JOURNAL OF PHYSICAL CHEMISTRY C · JANUARY 2010

Impact Factor: 4.77 · DOI: 10.1021/jp908319d

CITATION
1

READS
17

6 AUTHORS, INCLUDING:

Manuel Blázquez
University of Cordoba (Spain)
76 PUBLICATIONS **884** CITATIONS
SEE PROFILE

Rafael Madueño
University of Cordoba (Spain)
24 PUBLICATIONS **541** CITATIONS
SEE PROFILE

Teresa Pineda
University of Cordoba (Spain)
41 PUBLICATIONS **325** CITATIONS
SEE PROFILE

Luis Sánchez
University of Cordoba (Spain)
93 PUBLICATIONS **1,648** CITATIONS
SEE PROFILE

Available from: Rafael Madueño
Retrieved on: 01 February 2016

3D Gold Nanocrystal Arrays: A Framework for Reversible Lithium Storage

A. Viudez,[†] M. Blázquez,[†] R. Madueño,[†] J. Morales,[‡] T. Pineda,[†] and L. Sánchez*[,‡]

Departamento de Química Física y Termodinámica Aplicada and Departamento de Química Inorgánica e Ingeniería Química, Facultad de Ciencias, Campus de Rabanales, Edificio Marie Curie, Universidad de Córdoba, 14071 Córdoba, Spain

Received: August 10, 2009; Revised Manuscript Received: December 21, 2009

Nanosized metal particles are currently used in the development of high-capacity metal-based negative electrodes for Li-ion batteries. Here, we report on a new strategy that uses 6-mercaptopurine-monolayer protected gold clusters (6MP-MPCs) as an electrode for a lithium battery. The higher performance of the Li/6MP-MPC as compared to the Li/2D-Au cell (the latter consists of naked gold microparticles composed of nanocrystallites of around 17 nm in size) is explained on the basis of the three-dimensional organization of the 6MP-MPCs in the powder sample. The cell specific capacity of the Li/6MP-MPC is kept on extended cycling in contrast to the behavior observed for the Li/2D-Au cell that shows an abrupt decay of this magnitude after a few cycles. The reorganization of the 6MP molecular layer on the lithium−gold alloying process allows the accommodation of the increased cores in the same space volume, avoiding the cracks in the electrode, thus, keeping the electronic conduction.

Introduction

The increasing demand of high energy and power density for electronic portable devices has made new designs of lithium-ion batteries necessary. Thus, an intense research on materials for both positive and negative electrodes for these batteries has recently been developed. In the case of negative electrodes, the investigations have been focused on elements that alloy reversibly with Li (as are Si, Sn, and Sb) and show high gravimetric and volumetric capacities in comparison to graphite compounds that are commonly used in current commercial Li-ion batteries.[1] The main drawback for the implementation of these materials arises from the inhomogeneous volume expansions (up to 300%) associated with the electrochemical formation of the different Li_xM alloys.[2] This fact produces cracks on alloy grains and damages the electron transfer through the electrode and, hence, a rapid decline of delivered cell specific capacity is observed upon cycling.

An effective way of developing high-capacity metal-based negative electrodes is by the use of nanosized metal particles. Although this strategy generally results in an improved electrode electrochemical performance, recent studies have shown that reducing particle size does not suffice to ensure a consistently good electrochemical response from a lithium-alloy metal electrode during cycling.[3−5] Therefore, research into anode materials should go beyond the mere preparation of nanometric particles. Once the material volume expansion is reduced to the nanodomain by decreasing particle size, the next step should be to confine particles separately. In this way, contact between intermetallic particles while growing will be hindered and, thus, the formation of cracks in the electrode is avoided. Several successful strategies have been devoted to this by (i) embedding or encapsulating the metal nanoparticle into a matrix in order to construct a composite electrode,[6,7] (ii) dispersing nanoparticles with fibers[8−10] or binders,[11] and (iii) designing new architectures.[12−15]

In this paper, we present a new strategy that combines the above-mentioned points at nanoscale. We take advantage of the fact that the gold nanocrystals encapsulated by 6-mercaptopurine (6MP) molecules form a three-dimensional (3D) array and build an electrode to check its performance in a lithium ion battery. These gold nanoparticles are synthesized by using a derivation of the Brust method in one phase[16] by using 6MP as a protecting agent. The 6MP molecules bind to the gold nucleus surface through the mercapto group in a very short time, allowing the synthesis of gold clusters of a narrow distribution of sizes (2.4 ± 0.5 nm).[17]

Although the high cost and low specific capacity of gold makes it an unattractive metal to be used as an electrode for lithium batteries, the innovative synthetic methods for tailored gold nanoparticles have called our attention to test its electrochemical properties as a lithium alloying element. The promising results obtained in this work let us transfer this preparative methodology to more interesting electrode materials.

Experimental Section

Synthesis of 6MP-MPCs. Analytical grade 6-mercaptopurine, sodium borohydride, and dimethylformamide (Aldrich-Sigma), hydrogen tetrachloroaurate trihydrate (from 99.999% pure gold) prepared using a literature procedure,[18] and deionized water (18 MΩ) from milli-Q system were used in the experiments. All chemicals were used without further purification. The synthesis of 6MP-MPCs was made by following a variation of the single phase system first derived by Brust el al.[16] and is reported elsewhere as well as the nanoparticle characterization.[17]

Methods. HR-TEM images were obtained with a JEOL JEM 2010 instrument operating at 80−200 kV and analyzed using Image Pro Plus software. Samples were prepared by casting and evaporating a droptlet of MPC solution (2−3 mg/mL) onto Formvar-coated Cu grids (400 mesh, Electron Microscopy Sciences). SEM images were obtained on JEOL JSM-6400

* Corresponding author. Tel.: 34-957-218620. Fax: 34-957-218621. E-mail: luis-sanchez@uco.es.
[†] Departamento de Química Física y Termodinámica Aplicada.
[‡] Departamento de Química Inorgánica e Ingeniería Química.

10.1021/jp908319d © 2010 American Chemical Society
Published on Web 01/15/2010

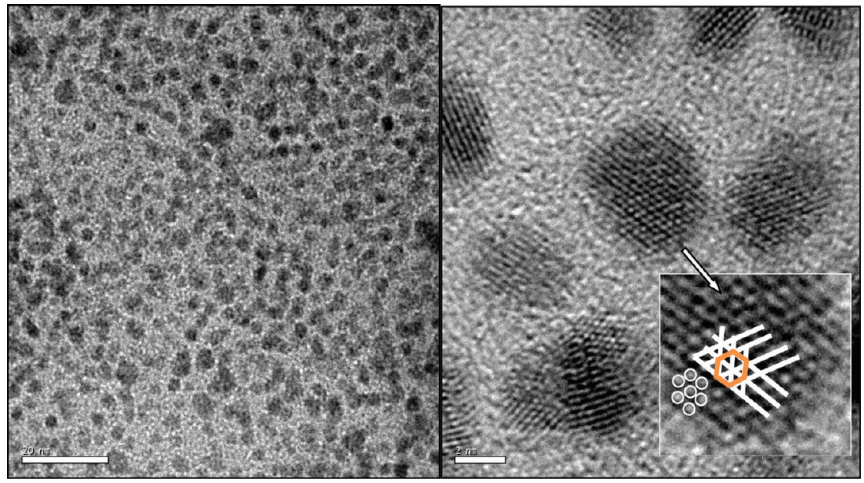

Figure 1. HR-TEM images of 6MP-MPCs. Scale bars are (left) 20 nm and (right) 2 nm. The inset shows the magnification of the nanocluster and the (111) arrangement of the gold atoms.

microscope, its accelerating voltage was 20 KV. X-ray powder diffraction (XRD) patterns were recorded on a Siemens D5000 X-ray diffractometer, using Cu Kα radiation and a graphite monochromator. The crystallite size was calculated by applying the Scherrer equation.[19]

Electrochemical measurements were performed in two electrode swagelok-type cells, using lithium as a counter-electrode. The electrolyte was Merck battery electrolyte LP 40 (EC:DEC = 1:1 w/w, 1 M $LiPF_6$) containing vinyl carbonate (VC) as an additive (2% by weight). Electrode pellets were prepared by pressing, in a stainless steel grid, about 2 mg of active material with polytetrafluoroethylene (5 wt %) and acetylene black (10 wt %) at 4 tons. Galvanostatic tests were conducted under a C/8 galvanostatic regime (C being defined as 1 Li^+ exchanged in 1 h). All electrochemical measurements were controlled via a MacPile II potentiostat-galvanostat.

Results and Discussion

The gold nanoclusters synthesized consist of a gold nucleus protected by a self-assembled monolayer of 6MP. This kind of nanostructure has been called monolayer-protected gold nanoclusters (MPCs)[20] and, only recently, a complete picture of its structure has been reported.[21,22] In fact, the complete structure determination of $Au_{102}(MBA)_{44}$ and $Au_{25}(SCH_2CH_2Ph)_{18}$ clusters has been obtained by X-ray crystallographic analysis, and it has been found that these nanostructures are composed of a central gold core protected by a "staple" motif of short, stellated semiring gold-thiolate chains.[22] Figure 1 shows the HR-TEM images of as-synthesized 6MP-monolayer protected gold clusters (6MP-MPCs). The high resolution images show well crystallized particles where the face-centered cubic (fcc) structure is easily visualized. A distance between the nearest neighbors of around 2.87 Å, which corresponds to gold atoms, is measured. The evidence for the presence of 6MP on the particle surface comes from FT-IR and XPS spectroscopies that show the binding of the organic molecule to the gold through the sulfur atom.[17] Moreover, a stoichiometry of $Au_{459}(6MP)_{62}$ has been determined for these nanoclusters based on thermogravimetric analysis and taking into account the average diameter of the gold nucleus of 2.4 ± 0.5 nm, determined by TEM. The main role of the 6MP monolayer adsorbed on the nanoparticle surface is the protection against aggregation in solution[17,23] as well as in the dry solid sample.[20] However, the 6MP monolayer does not inhibit the electronic conduction.[17,24,25] In fact, the mediator role of the 6MP molecule in electron transfer processes has long been recognized.[25−27]

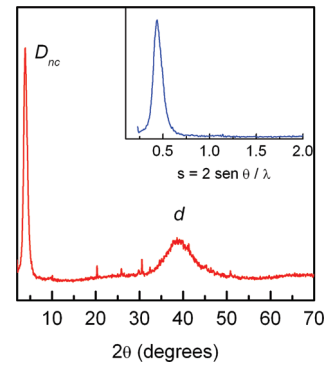

Figure 2. XRD pattern of the 6MP-MPC sample. The inset shows the small-angle region.

The powder X-ray diffractogram of the 6MP-MPCs (Figure 2) shows a broad peak at 38.9° consistent with the (111) reflection line for Au (ICDD card n° 4−784). However, in a deeper examination, a shoulder at higher reflection angles, that is 45.5°, coinciding to the (200) reflection line can be observed. The peak width (after deconvolution of the signal by two Gaussian-shaped peaks centered at 38.2 and 44.4° and corrected by instrumental broadening) allows the determination of a cluster size of 1.9 nm by using the Scherrer formula.[28] This size is lower than the value obtained by TEM, although differences of this kind are usually found when the sizes are measured by TEM[29] and mass spectrometry[30] techniques. Several narrow and low intense signals show the presence of a small amount of crystalline impurities that can be ascribed to Au_2S[31] that can be formed in the nanoclusters synthesis process or originated from decomposition. An interesting finding is the presence of the intense signal at small reflection angles. The pattern of strong and sharp peaks obtained for some large molecules in the small-angle region is interpreted as a lattice packing into ordered arrays. However, the observation of such a pattern depends on the purity of the material. Thus, in the absence of such a pattern, the position of the first reflection peak can be used to obtain the structural parameter D_{nc}, that is, the nanocrystal center-to-center nearest-neighbor distance (Scheme 1).[32] A value of 2.85 nm can be determined that, taking into account the gold nucleus diameter as measured by large-angle XRD, gives a distance between each neighboring cluster core of 0.95 nm. This distance is lower than twice that of the 6MP molecule (i.e., monolayer thickness: 0.6−0.8 nm), consistent with the organization found in other clusters[32−35] as well as in molecular

SCHEME 1: Ideal Representation of the 6MP-MPCs in the Solid Crystalline State

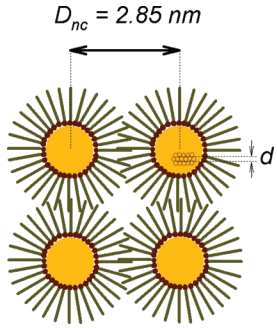

dynamics simulations of larger cluster compounds,[36] which implies a significant overlap of the passivating layers in the condensed form. This cluster's assembly is an interesting structure that can be used to enhance the electrochemical properties of gold as anode material for lithium batteries, taking advantage of the separation between the gold cores that could absorb the volume expansion when Au is converted to Li_xAu during the electrochemical process, thus, avoiding the mechanical material deterioration.

The electrochemical response of the sample was measured in a two-electrode Li/$LiPF_6$ EC-DEC (2% VC)/6MP-MPC. The cell was cycled over the voltage range 1.1−0.0 V. The first three cycles are shown in Figure 3a. Three potential steps were observed on the first discharge curve at 1.6−1.0, 1.0−0.25, and <0.25 V. For comparison, a similar test was performed with an electrode made of massive gold as the active material (Figure 3b). This sample was obtained by the homogeneous reduction of an $AuCl_4^-$ acidic solution with $[NH_4]_2[Fe][SO_4]_2 \cdot 6H_2O$. The gold crystallized in a two-dimmensional (2D) nanostructured material with a crystallite size of around 17 nm. For this electrode, 2D-Au, the first discharge curve consisted of two well-defined plateaus at 0.25 and 0.1 V that consume 3.25 faradays·mol^{-1}. Assuming that gold can electrochemically alloy with lithium reaching the $Li_{15}Au_4$ stoichiometry in the two systems, the different shape and extension of the first discharge curve indicates that a secondary reaction takes place in the Li/6MP-MPC cell. Additional information was obtained from the step potential electrochemical scanning curves (see Supporting Information). The processes such as water traces, solvent and salt anions reduction (the latter leads to a solid electrolyte interface (SEI) film), and lithium underpotential deposition (upd) result are more significant for the 6MP-MPC electrode. In this sense, it must be taken into account that a higher catalytic activity has been reported for nanometric gold particles.[37] Thus, the difference between gold nanoparticles and extended gold surfaces can be explained by considering the metal coordination number of the gold atoms to which the reactants can be bound. While gold atoms on a close-packed surface have nine neighbors, those at step and at corner sites of the small particles can have only three or four. Smaller particles (<2.5 nm) have a larger number of low-coordinated gold atoms located at the edges that, on the other hand, are easily accessible to reactant molecules. This fact supports the hypothesis that the 6MP-MPC electrode would exhibit catalytic activity toward the observed side electrochemical reactions and explains the large extension of the first discharge curve. Because some of these electrochemical processes are irreversible, the subsequent charge/discharge curves result in a similar extension for the two studied electrodes. In these cases, the consumption (in faradays·mol^{-1}) is lower than 2.0, indicating that Li_xAu compounds within the

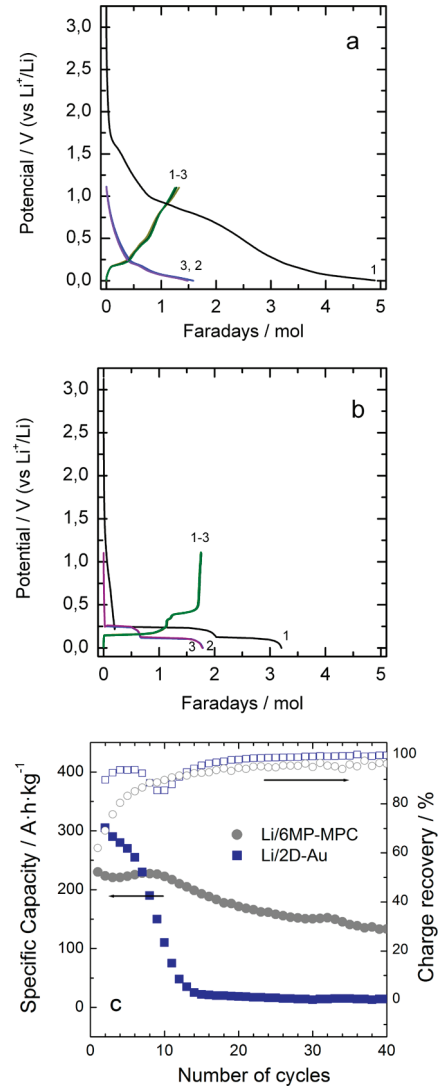

Figure 3. Charge/discharge voltage profiles of the (a) 6MP-MPC and (b) 2D-Au electrodes cycled between 1.1 and 0.0 V (vs Li/Li^+). (c) The delivered specific discharge capacities and charge recovery values of the 6MP-MPC (●,○) and 2D-Au (■,□) electrodes according to the cycle number. Capacity values are referred to gold mass in both electrodes.

range of $Li_{0.4}Au_{0.6}$, LiAu, Li_3Au, $Li_{15}Au_4$ alloys are formed.[14,38,39] It is worth mentioning the different slopes observed in the charge/discharge step potentials. The smooth curves observed for the Li/6MP-MPC cell indicate the formation of a single active solid matrix. In contrast, the appearance of well-defined potential steps in the case of the Li/2D-Au system is typical for the formation of two-phase regions. The appearance of single phase Li extraction/insertion behavior would be related with the reduction in particle size, as it has been previously reported for the $LiFePO_4$ system.[40]

Figure 3c shows the variation of the cell specific capacity and charge recovery values with the number of cycles for the Li/6MP-MPC and Li/2D-Au systems. The initial capacity values for 6MP-MPC were lower than those observed for 2D-Au. As commented before, these could be associated with the existence of irreversible secondary processes on the 6MP-MPC electrode. In fact, a low charge recovery was obtained for the first cycles. Nevertheless, the reversibility of the electrochemical process enhanced with extended cycling. Capacity retention was quite good for 6MP-MPC: an average of 170 mAh/g was maintained on extended cycling. Conversely, the capacity abruptly faded (below 20 mAh/g at the fifteenth cycle) in the case of 2D-Au.

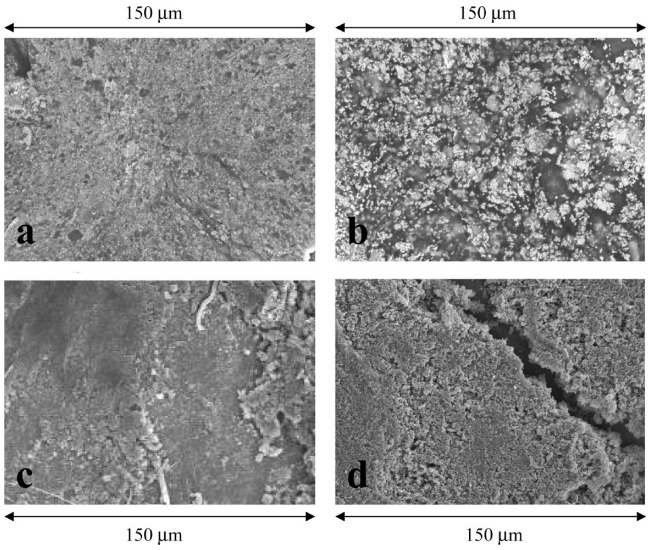

Figure 4. SEM images of 6MP-MPC (left) and 2D-Au (right) electrodes before the electrochemical process (a,b) and after extended cycling (c,d).

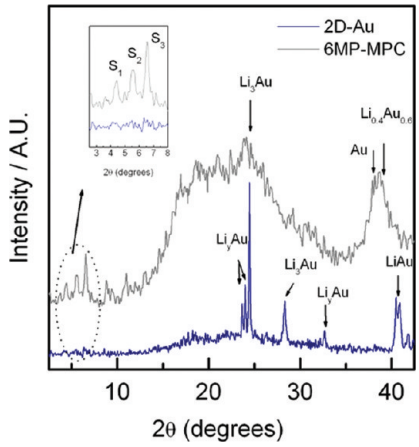

Figure 5. XRD pattern of the electrodes after the first discharge curve.

The lithium alloying process involves a large increase of volume; the increasing factors per mol of Au are 1.74 and 3.68 for LiAu and Li_3Au alloys, respectively. These changes induce mechanical stress in the particles that cause cracks.

This phenomenon is clearly observed in the SEM images obtained for electrodes. Figure 4 shows the surface morphology of electrodes as prepared (a, b) and after extended cycling (c, d). The four images show the powdery nature of the active material. The most significant feature is the apparition of big cracks on the 2D-Au electrode after cycling, while the surface of the 6MP-MPC electrode is practically unaltered. This feature hinders the electronic conduction in the 2D-Au electrode, composed of larger and naked particles, and its electrochemical performance becomes very poor. However, the peculiar nanometric 3D structure of the 6MP-MPC sample serves to circumvent this problem.

To gain more insight into the knowledge of this electrochemical behavior, the XRD patterns of the sample after the first discharge curve were recorded (Figure 5a). For the 2D-Au sample, several narrow diffraction peaks were identified with the presence of lithium gold alloys, Li_3Au (ICDD card No. 65-8632), LiAu (ICDD card No. 50-1035), and Li_yAu,[39] being the former predominant one. The assigning of the phases for the XRD pattern of the discharged 6MP-MPC electrode was more difficult. In this case, the low crystalline structure of the sample together with the necessity of a polyethylene protective film to cover the sample (broad signal in the 15−30° range) and the presence of a SEI film in the surface preclude the observation of some diffraction lines expected for lithium gold alloys. However, the positions of the broad peaks are in agreement with the formation of Li_3Au and $Li_{0.4}Au_{0.6}$ alloys whose highest reflections occur at 24.5° [ICDD card No. 65-8630] and 39.5°,[39] respectively. The latter has a significant contribution of the gold (111) diffraction line (at 38.2°), indicating that some gold particles have remained inactive. This can be a consequence of the electrochemical side reactions that consume some amounts of current in addition to that for the formation of lithium alloys during the first electrochemical cycle. Nevertheless, the most interesting feature of this XRD pattern is found in the small-angle region. Three small and narrow reflections, denoted as S_1, S_2, and S_3 at 4.46, 5.60, and 6.63°, respectively, were always present in

SCHEME 2: Illustration of the Changes in the Electrode Structures after the Charge/Discharge Processes and Subsequent Core Size Increases: (Top) 2D-Au and (Bottom) 6MP-MPC

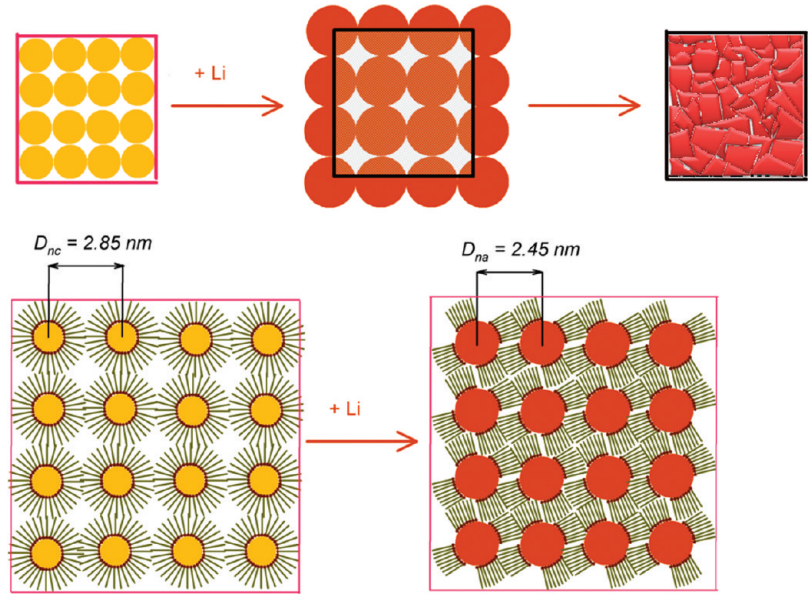

the XRD patterns of the repeated samples but absent for the discharged 2D-Au electrode (see also the inset of Figure 5).

The differences found in the structure of the lithiated products as well as the electrochemical performance of the two systems indicate that the alloying mechanism was substantially influenced by the presence of a 3D nanoparticles arrangement in the 6MP-MPC sample. Scheme 2 shows a schematic illustration of the lithium reaction mechanism by considering the gold cores, with or without the 6MP shell, in a square confinement. The naked gold particles suffer a great increase in volume upon alloy with lithium that makes them expand out the square confinement. However, the expansion process is restricted due to the 3D rigid conglomeration of the particles in a powder sample. Then, the alloy particles are not free to expand and the spatial confinement force them to crack (Scheme 2).

The 3D arrangement of the 6MP-MPCs offers a different scenario with lower gold cores spatial density. The square confinement, due to the presence of the 6MP monolayer protecting the gold MPCs, is larger and could easily absorb the core volume expansion. The area of the metallic cores increases and the surface coverage of the 6MP molecules changes leading to an uneven molecular distribution. This fact should provoke a reorganization of the molecules in "*bundles*", leaving areas of lower density that help to accommodate the nanoparticles in the spatial confinement.[41] Thus, this simple illustration serves to show that expanded Li_x(6MP-MPC) particles can be limited at the pristine square confinement, without cracking, when a well established arrangement of 6MP shell's organic groups occurs. Therefore, the spatial order of nanocrystal changes and, after the reaction with lithium, they are separated by a distance, D_{na}, which is shorter than D_{nc} (Scheme 2). This fact is supported by the evidence found on the Li_x(6MP-MPC) XRD pattern, in which diffraction peaks in the small-angle region (S_1, S_2, S_3) are present, indicating the existence of a different superstructure. Thus, an interplanar distance of 2.45 nm was found for the first diffraction line that was smaller than D_{nc} of 2.85 nm.

In summary, the 3D arrangement of 6MP-MPCs has some influences on the electrochemical properties of gold as anode material for lithium batteries. The 6MP-MPC electrode showed a good retention of the specific capacity delivered values of about 180 mAh/g on extended cycling. Conversely, the capacity faded abruptly in the case of a standard Au electrode. Moreover, significant differences were found for the structural analysis of the lithiated products, showing the Li_x(6MP-MPC) sample several diffraction peaks in the small-angle region that indicate that the 3D molecular array is maintained for the alloy particles. The enhanced buffer action of 3D-6MP-MPC matrix to accommodate volume expansions in comparison to that exhibited in the 2D-Au, together with the difference of particle size, are designed as responsible for the good electrochemical properties observed. This innovative strategy leading to the enhancement of the electrochemical performance of a metallic anode material should be potentially applicable to more interesting materials (vg. Si or Sn) in the field of Li-ion batteries.

Acknowledgment. We thank the Ministerio de Educación y Ciencia (MEC; Projects MAT2005-03069 and CTQ2007-62723/BQU), Junta de Andalucía (Groups FQM-111 and -175), and University of Córdoba for financial support of this work. A.J.V. acknowledges the MEC for a fellowship of the FPU program.

Supporting Information Available: Additional electrochemical tests. This material is available free of charge via the Internet at http://pubs.acs.org.

References and Notes

(1) Idota, Y.; Kubota, T.; Matsufuji, A.; Maekawa, Y.; Miyasaka, T. *Science* **1997**, *276*, 1395.
(2) Beaulieu, L. Y.; Eberman, K. W.; Turner, R. L.; Krause, L. J.; Dahn, J. R. *Electrochem. Solid-State Lett.* **2001**, *4*, A137.
(3) Zhang, T.; Gao, J.; Zhang, H. P.; Yang, L. C.; Wu, Y. P.; Wu, H. Q. *Electrochem. Commun.* **2007**, *9*, 886.
(4) Larcher, D.; Beattie, S.; Morcrette, M.; Edstroem, K.; Jumas, J. C.; Tarascon, J. M. *J. Mater. Chem.* **2007**, *17*, 3759.
(5) Martin, F.; Morales, J.; Sanchez, L. *ChemPhysChem* **2008**, *9*, 2610.
(6) Bryngelsson, H.; Eskhult, J.; Nyholm, L.; Herranen, M.; Alm, O.; Edstrom, K. *Chem. Mater.* **2007**, *19*, 1170.
(7) Lee, H.; Cho, J. *Nano Lett.* **2007**, *7*, 2638.
(8) Caballero, A.; Morales, J.; Sanchez, L. *Electrochem. Solid-State Lett.* **2005**, *8*, A464.
(9) Caballero, A.; Morales, J.; Sanchez, L. *J. Power Sources* **2008**, *175*, 553.
(10) Carmer, J. L. G.; Morales, J.; Sanchez, L. *Electrochem. Solid-State Lett.* **2008**, *11*, A101.
(11) Li, J.; Lewis, R. B.; Dahn, J. R. *Electrochem. Solid-State Lett.* **2007**, *10*, A17.
(12) Peng, K.; Jie, J.; Zhang, W.; Lee, S. T. *Appl. Phys. Lett.* **2008**, *93*, 33105.
(13) Kim, D. W.; Hwang, I. S.; Kwon, S. J.; Kang, H. Y.; Park, K. S.; Choi, Y. J.; Choi, K. J.; Park, J. G. *Nano Lett.* **2007**, *7*, 3041.
(14) Chan, C. K.; Peng, H. L.; Liu, G.; McIlwrath, K.; Zhang, X. F.; Huggins, R. A.; Cui, Y. *Nat. Nanotechnol.* **2008**, *3*, 31.
(15) Ning, J. J.; Jiang, T.; Men, K. K.; Dai, Q. Q.; Li, D. M.; Wei, Y. J.; Liu, B. B.; Chen, G.; Zou, B.; Zou, G. T. *J. Phys. Chem. C* **2009**, *113*, 14140.
(16) Brust, M.; Fink, J.; Bethell, D.; Schiffrin, D. J.; Kiely, C. *J. Chem. Soc., Chem. Commun.* **1995**, 1655.
(17) Viudez, A. J.; Madueno, R.; Blazquez, M.; Pineda, T. *J. Phys. Chem. C* **2009**, *113*, 5186.
(18) Brauer, G. *Handbook of Preparative Inorganic Chemistry*; Academic Press: New York, 1965.
(19) Klug, H. P.; Alexander, L. E. *X-Ray Diffraction Procedures for Polycrystalline and Amorphous Materials*; Wiley: New York, 1974.
(20) Templeton, A. C.; Wuelfing, M. P.; Murray, R. W. *Acc. Chem. Res.* **2000**, *33*, 27.
(21) Jadzinsky, P. D.; Calero, G.; Ackerson, C. J.; Bushnell, D. A.; Kornberg, R. D. *Science* **2007**, *318*, 430.
(22) Heaven, M. W.; Dass, A.; White, P. S.; Holt, K. M.; Murray, R. W. *J. Am. Chem. Soc.* **2008**, *130*, 3754.
(23) Viudez, A. J.; Madueno, R.; Pineda, T.; Blazquez, M. *J. Phys. Chem. B* **2006**, *110*, 17840.
(24) Madueno, R.; Sevilla, J. M.; Pineda, T.; Roman, A. J.; Blazquez, M. *J. Electroanal. Chem.* **2001**, *506*, 92.
(25) Madueno, R.; Garcia-Raya, D.; Viudez, A. J.; Sevilla, J. M.; Pineda, T.; Blazquez, M. *Langmuir* **2007**, *23*, 11027.
(26) Pineda, T.; Sevilla, J. M.; Roman, A. J.; Blazquez, M. *Biochim. Biophys. Acta, Protein Struct. Mol. Enzymol.* **1997**, *1343*, 227.
(27) Sevilla, J. M.; Pineda, T.; Roman, A. J.; Madueno, R.; Blazquez, M. *J. Electroanal. Chem.* **1998**, *451*, 89.
(28) Klug, H. P.; Alexander, L. E. *X-Ray Diffraction Procedures for Polycrystalline and Amorphous Materials*; Wiley: New York, 1974.
(29) Solliard, C. *Surf. Sci.* **1981**, *106*, 58.
(30) Vezmar, I.; Alvarez, M. M.; Khoury, J. T.; Salisbury, B. E.; Shafigullin, M. N.; Whetten, R. L. *Z. Phys. D: At., Mol. Clusters* **1997**, *40*, 147.
(31) Ishikawa, K.; Isonaga, T.; Wakita, S.; Suzuki, Y. *Solid State Ionics* **1995**, *79*, 60.
(32) Schaaff, T. G.; Shafigullin, M. N.; Khoury, J. T.; Vezmar, I.; Whetten, R. L. *J. Phys. Chem. B* **2001**, *105*, 8785.
(33) Schaaff, T. G.; Shafigullin, M. N.; Khoury, J. T.; Vezmar, I.; Whetten, R. L.; Cullen, W. G.; First, P. N.; GutierrezWing, C.; Ascensio, J.; JoseYacaman, M. J. *J. Phys. Chem. B* **1997**, *101*, 7885.
(34) Whetten, R. L.; Khoury, J. T.; Alvarez, M. M.; Murthy, S.; Vezmar, I.; Wang, Z. L.; Stephens, P. W.; Cleveland, C. L.; Luedtke, W. D.; Landman, U. *Adv. Mater.* **1996**, *8*, 428.
(35) Whetten, R. L.; Shafigullin, M. N.; Khoury, J. T.; Schaaff, T. G.; Vezmar, I.; Alvarez, M. M.; Wilkinson, A. *Acc. Chem. Res.* **1999**, *32*, 397.
(36) Luedtke, W. D.; Landman, U. *J. Phys. Chem.* **1996**, *100*, 13323.
(37) Hvolbaek, B.; Janssens, T. V. W.; Clausen, B. S.; Falsig, H.; Christensen, C. H.; Norskov, J. K. *Nano Today* **2007**, *2*, 14.
(38) Dey, A. N. *J. Electrochem. Soc.* **1971**, *118*, 1547.
(39) Taillades, G.; Benjelloun, N.; Sarradin, J.; Ribes, M. *Solid State Ionics* **2002**, *152*, 119.
(40) Gibot, P.; Casas-Cabanas, M.; Laffont, L.; Levasseur, S.; Carlach, P.; Hamelet, S.; Tarascon, J. M.; Masquelier, C. *Nat. Mater.* **2008**, *7*, 741.
(41) Love, J. C.; Estroff, L. A.; Kriebel, J. K.; Nuzzo, R. G.; Whitesides, G. M. *Chem. Rev.* **2005**, *105*, 1103.

JP908319D